Novel superhard tetragonal hybrid sp^3/sp^2 carbon allotropes C_x (x = 5, 6, 7): Crystal chemistry and ab initio studies

Samir Matar, Vladimir Solozhenko

Novel superhard tetragonal hybrid sp^3/sp^2 carbon allotropes C_x (x = 5, 6, 7): Crystal chemistry and *ab initio* studies

Samir F. Matar https://orcid.org/0000-0001-5419-358X
Lebanese German University (LGU), Jounieh, P.O. Box 206, Lebanon

Vladimir L. Solozhenko* https://orcid.org/0000-0002-0881-9761
LSPM–CNRS, Université Sorbonne Paris Nord, 93430 Villetaneuse, France

Abstract

Novel superhard tetragonal carbon allotropes C_5, C_6, and C_7, characterized by the presence of sp^3- and sp^2-like carbon sites, have been predicted from crystal chemistry and extensively studied by quantum density functional theory (DFT) calculations. All new allotropes were found to be cohesive, with crystal densities and cohesive energies decreasing along the C_5-C_6-C_7 series due to the greater openness of the structures resulting from the presence of C=C ethene and C=C=C propadiene subunits, and mechanically stable with positive sets of elastic constants. The Vickers hardness evaluated by different models qualifies all allotropes as superhard with H_v values ranging from 90 GPa for C_5 to 79 GPa for C_7. Phonon band structures confirm that the new allotropes are also dynamically stable. The electronic band structures reveal their metallic-like behavior due to the presence of sp^2-hybridized carbon.

***Keywords*:** carbon allotropes; DFT; topology; crystal structure; equation-of-state; elastic constants; hardness; phonons; electronic band structures

* Corresponding author (vladimir.solozhenko@univ-paris13.fr)

1. Introduction

In recent years, significant efforts in the search for novel phases with advanced properties have benefited from structure prediction programs such as USPEX [1] and CALYPSO [2], and more recently from the crystallographic machine learning platform *CrystalMELA* [3]. The topic of carbon research, especially regarding periodic structures, shows a sustained interest in the search for new allotropes, especially those characterized by ultrahigh hardness close to that of diamond. In view of the large number of carbon structures claimed as novel, a database SACADA [4] has been created to group all known carbon allotropes, thus helping researchers in their endeavors on the one hand, and avoiding claims of known phases as novel allotropes on the other.

Another avenue of investigation that could be complementary to modern materials science software lies in the crystal chemistry rationale called "structural engineering". Recently, the body-centered tetragonal *tet*-C_4 (Fig. 1a) in space group *I*-4*m*2 was proposed by us as one of the simplest three-dimensional (3D) carbon networks to serve as a template for the design of other novel allotropes and chemical compounds [5]. Using the TopCryst crystallography package [6], *tet*-C_4 was identified with **dia** (i.e. diamond-like) topology. Several chemical compounds also have a **dia** topology, as categorized in the Reticular Chemistry Structure Resource (RCSR) database [7].

Recently, Wei *et al.* proposed a superhard *tet*-C_5 allotrope with mixed carbon hybridization (sp^2 and sp^3) and metallic character based on structure prediction programs and first-principles calculations within DFT [8]. However, such 'pentacarbon' should be unstable because it has some negative elastic constants. Later, in 2020, cubic 'pentadiamond' was reported as a novel allotrope with mechanical properties close to diamond, but the paper was retracted due to serious errors in the optimized structure of 'pentadiamond' under mechanical deformation admitted by the authors themselves [9]. Such interest in C_5 allotropes with mixed carbon hybridization arises from the possible change of the electronic structure of insulating diamond, leading to metallic-like behavior with potential applications in electronics [10].

In the present work, starting from *tet*-C_4 [5], we construct novel tetragonal carbon allotrope C_5 by crystal chemistry modifications followed by full geometry relaxations using calculations based on the quantum mechanics density functional theory DFT [11,12]. The proposed *tet*-C_5 was found to be cohesive and stable both mechanically and dynamically, and exhibit an original undocumented topology. In a subsequent step, new tetragonal C_6 and C_7 allotropes were proposed and analyzed simultaneously with *tet*-C_5. From a chemical point of view, C_5 and C_6 emphasize the double bond >C=C< *ene*, as in the ethene molecule, C_2H_4. Remarkably linear *C3* >C=C=C< resembling the allene or *propadiene* molecule, C_3H_4, characterize C_7.

After this contextual introduction and Section 2, which presents the computational framework, the crystal chemistry rationale leading to the novel tetragonal C_5, C_6 and C_7 allotropes is discussed. Section 3 is devoted to the crystal engineering protocol used to develop the various allotropes. Section 4 qualitatively illustrates the charge density projections on and between the

atoms. The mechanical, dynamic and thermal properties are detailed in Sections 5, 7 and 8, respectively, and the electronic band structures are discussed in Section 9.

2. Computational framework

The structural investigations using structure prediction programs [1-3] or requiring crystal engineering as here, need quantitative support from quantum mechanical calculations. Such investigations are mostly carried out within the framework of DFT [11,12], which is widely accepted by the scientific community. Briefly, the DFT was developed in two works: for the theoretical framework by Hohenberg and Kohn in 1964 [11], then followed by Kohn and Sham in 1965 [12], who established the Kohn-Sham equations for solving the wave equation practically within computational codes built around the DFT. The Vienna Ab initio Simulation Package (VASP) code [13,14] and the Projector Augmented Wave (PAW) method [14,15] for the atomic potentials were used for the identification of the ground state structures corresponding to the energy minima and the subsequent prediction of their mechanical and dynamical properties. DFT exchange-correlation (XC) effects were considered using the generalized gradient approximation (GGA) [16]. Relaxation of the atoms to the ground state structures was performed with the conjugate gradient algorithm according to Press *et al*. [17]. The Blöchl tetrahedron method [18] with corrections according to the Methfessel and Paxton scheme [19] was used for geometry optimization and energy calculations, respectively. Brillouin-zone (BZ) integrals were approximated by a special **k**-point sampling according to Monkhorst and Pack [20]. Structural parameters were optimized until atomic forces were below 0.02 eV/Å and all stress components were < 0.003 eV/Å^3. The calculations were converged at an energy cutoff of 400 eV for the plane-wave basis set in terms of the **k**-point integration in the reciprocal space from *kx*(6)×*ky*(6)×*kz*(6) up to *kx*(12)×*ky*(12)×*kz*(12) to obtain a final convergence and relaxation to zero strains for the original stoichiometries presented in this work. In the post-processing of the ground state electronic structures, the charge density projections were operated on the lattice sites.

The mechanical stability criteria were obtained from the calculations of the elastic constants. The treatment of the results was done using the ELATE online tool [21], dedicated to the analysis of the elastic tensors. The program provides the bulk (*B*), shear (*G*) and Young's (*E*) moduli along different averaging methods; here the Voigt method [22] was used. Two empirical models, Mazhnik-Oganov [23] and Chen-Niu [24], have been used to estimate Vickers hardness (H_V) from elastic constants.

Vickers hardness was also evaluated in the framework of the thermodynamic model [25,26], which is based on thermodynamic properties and crystal structure, and using the Lyakhov-Oganov approach [27], which takes into account the topology of the crystal structure, the strength of covalent bonds, the degree of ionicity, and directionality. The fracture toughness (K_{Ic}) was estimated using the Mazhnik-Oganov model [23].

The dynamic stabilities of the new allotropes were confirmed by the positive values of the phonon frequencies. The corresponding phonon band structures were obtained from a high resolution of the tetragonal Brillouin zones according to Togo *et al*. [28]. The electronic band structures were obtained using the all-electron DFT based ASW method [29] and the GGA XC functional [16]. The VESTA (Visualization for Electronic and STructural Analysis) program [30] was used to visualize the crystal structures and charge densities.

3. Crystal structure engineering

The template *tet*-C_4 (space group *I*-4*m*2, No. 119) is characterized by two 2-fold Wyckoff atomic positions for carbon as shown in Table 1 [5]. The tetragonal body-centered structure in Fig. 1a shows the corresponding carbon atoms labeled C1 (brown spheres) at the origin and body center and C2 (white spheres) forming tetrahedra around C1. Considering the structure in the simple tetragonal configuration, the second column of Table 1 explains the four carbon sites. The transformation to C_5 retains the tetragonal symmetry, albeit lowered from body-centered ("I" centering) to primitive ("P" centering) and resolved in space group *P*-4*m*2, No. 115. This consists in keeping the body-centered carbon (C1 at ½, ½, ½) so that it becomes in C(1c) Wyckoff position – follow the transformation arrows – as well as the two C2s (C2a and C2b) become C3(2g) where the z coordinate becomes ±z′ instead of ±¼. The additional carbon C2 is provided by parameterizing the z position of C1b, resulting in a two-fold C2 (2e) at 0, 0, ±z. After full geometry relaxation, the resulting structure is shown in Fig. 1b with colored spheres corresponding to the three carbon sites given with the coordinates in Table 1, i.e. with well determined z = ±0.854 and z′ = ±0.314. The topology of *tet*-C_5 is found to be **3,4^2T1-CA**, documented in the SACADA database, while the template *tet*-C_4 has a **dia** topology. Now the cohesive energy per atom: E_{coh}/atom = -2.06 eV is lower than that of *tet*-C_4, which is characterized by a large cohesive energy E_{coh}/atom = -2.49 eV (the same as in diamond).

The polyhedral projection of the *tet*-C_5 structure (Fig. 2a, center) shows four tetrahedra. More details are observed in the right panel of Fig. 2a with a double cell along the *c*-direction, highlighting the C2-C2 bonds between the tetrahedra in these two cells. The C2-C2 segments form double bonds like C=C *ene* units, which will be further discussed in Section 4 relevant to the charge density projections.

Using *tet*-C_5 as a template, a new tetragonal C_6 allotrope was constructed with the modification of the central carbon position from ½, ½, ½ to ½, ½, z with z ~ 0.4, thus transforming it into a two-fold position (2f) in the primitive tetragonal space group *P*-4*m*2, No. 115. However, after full geometry optimization, and space group analysis, the (2e) and (2f) positions were merged by symmetry into a single four-fold position with body-center space group *I*-4*m*2, No. 119, as shown in Table 2. The topological analysis of the new allotrope revealed a **tfa** topology similar to that of the recently reported ultrahard C_6 allotrope called 'neoglitter' [31]. The cohesive energy of the new *tet*-C_6 is E_{coh}/atom = -1.73, which allows us to describe it as cohesive but less stable

than *tet*-C_5. The structure of *tet*-C_6 is shown in Fig. 2b in three representations. Clearly, the tetrahedra are now connected by C2-C2 segments along two adjacent as in C_5 but also within the cell, thus exhibiting the higher symmetry compared to *tet*-C_5.

The addition of a central carbon atom to *tet*-C_6 results in C_7 stoichiometry. The fully geometry-optimized lattice parameters are given in Table 2. There are now 4 different Wyckoff positions in the primitive tetragonal space group *P*-4*m*2, No. 115. The topological analysis led to the assignment of **tfa** topology as in the case of *tet*-C_5. The structure of *tet*-C_7 is shown in Fig. 2c, with the aligned C=C=C connecting the tetrahedra within the cell. As in C_5 and C_6, two adjacent cells are connected via C2-C2. However, *tet*-C_7 has the exception of having both C=C *ene* and C=C=C propadiene subunits. The cohesive energy E_{coh}/atom = -1.69 eV is lower than that of *tet*-C_6.

The density changes drastically along the series: $\rho(C_5) = 3.25 > \rho(C_6) = 3.12 > \rho(C_7) = 2.84$ g/cm^3 due to the increase in volume caused by the introduction of a larger number of sp^2-hybridized carbon atoms into the unit cell. The shortest interatomic distance (1.30 Å) is observed in the case of C_7 for the propadiene-like C=C=C subunit, whereas in C_6 d(C=C) = 1.44 Å. The other distances shown in Table 2 are in the range of values observed for tetrahedral carbon allotropes. The relevant effects on the phonon frequencies are shown in Section 7.

Simulated X-ray diffraction patterns of three new tetragonal carbon allotropes are shown in Fig. 3. It is evident that they all exhibit distinct topologies that differ significantly from diamond.

4. Projections of the charge densities

To illustrate the peculiarities introduced by the C=C and C=C=C subunits into the lattice, the analysis was extended to a qualitative illustration of the charge densities. Despite the similar chemical nature of the constituents, i.e. carbon, the different hybridizations (sp^3 and sp^2) lead to different behaviors of the carbon sites in terms of charge transfer. Fig. 4 illustrates the charge density distribution.

The most relevant feature in C_5 (Fig. 4a) is the red charge cross sections, which indicate the continuous charge density of the red traces through the 8 corners toward the adjacent cells along the tetragonal *c* direction (vertical direction). This feature is also observed within the C_6 cell, which shows similar to C_5 features regarding the 8 corners, as well as the central >C=C< with characteristic sp^2 hybridization. Going to C_7, the central part of the unit cell contains the >C=C=C< propadiene subunit, while the >C=C< *ene* subunits are located between the two adjacent cells (Fig. 4c). However, the charge density becomes weaker as you move to the next cell, as shown by the green areas, which indicate less charge between adjacent cells; the charge is now concentrated around the propadiene subunit. This may explain why C_7 is the least cohesive of the series studied.

5. Mechanical properties

An analysis of the mechanical behavior of new tetragonal carbon allotropes has been carried out by calculating the elastic properties by inducing finite distortions of the lattice. The allotropes are fully described by the calculated sets of elastic constants C_{ij} given in Table 3. All C_{ij} values are positive, indicating mechanically stable phases. The major (i.e., C_{11} and C_{33}) C_{ij} values of C_5 are systematically larger than those of C_6 and C_7. The analysis of the elastic tensors was performed using the ELATE software [21], which provides the bulk (*B*), shear (*G*) and Young's (*E*) moduli, and the Poisson's ratio (ν) along different averaging methods; in the present work, the Voigt approach [22] was chosen. Table 4 shows the calculated elastic moduli, with values that follow the trends observed for C_{ij}.

The Vickers hardness values evaluated using the four contemporary hardness models are summarized in Table 4. A clear tendency of a decrease in hardness in the C_5–C_6–C_7 series due to the increasing openness of the crystal structures is observed for all four models. Since it has been shown earlier that the thermodynamic model is the most reliable in the case of the superhard compounds of light elements [33] and shows perfect agreement with the available experimental data [34], it is obvious that the hardness values calculated within the empirical models are strongly underestimated. The Oganov-Lyakhov model also gives underestimated (by 10-20%) values.

The fracture toughness of the new carbon allotropes decreases from 7.1 $MPa \cdot m^{1/2}$ for *tet*-C_5, which is higher than that of diamond (K_{Ic} = 6.7 $MPa \cdot m^{1/2}$ [35]), down to 5.8 $MPa \cdot m^{1/2}$ for *tet*-C_7.

6. Equations of state

The comparative energy trends of new tetragonal carbon allotropes have been determined from their equations of state, based on a series of calculations of total energy as a function of volume. The resulting *E*(V) curves fitted to the third-order Birch equations of state [36] are shown in Fig. 5. As can be seen, all three tetragonal carbon allotropes are metastable over the entire range of experimentally accessible pressures. However, the formation of these allotropes is possible at high pressures and high temperatures as a result of alternative metastable behavior, most likely under highly non-equilibrium conditions.

7. Phonon band structures

To verify the dynamic stability of the novel carbon allotropes, their phonon properties were studied. The phonon band structures obtained from a high resolution of the tetragonal Brillouin zone according to Togo *et al*. [28] are shown in Fig. 6. The bands (red lines) develop along the main directions of the tetragonal Brillouin zone (horizontal *x*-axis), separated by vertical lines for

better visualization, while the vertical direction (*y*-axis) shows the frequencies ω, given in terahertz (THz).

The band structures include 3N bands: three acoustic modes starting from zero energy (ω = 0) at the Γ point (the center of the Brillouin zone) up to a few terahertz, and 3N-3 optical modes at higher energies. The acoustic modes correspond to the rigid translation modes of the crystal (two transverse and one longitudinal). All panels in Fig. 6 show positive phonon frequencies, indicating the dynamic stability of all three new carbon allotropes.

In Fig. 6a, relevant to C_5, the general aspect is that of dispersed bands with the highest magnitude just below 40 THz. This changes for C_6 (Fig. 6b), where the highest frequency is closer to 40 THz, corresponding to 1650 cm^{-1}. This value is exactly in the range of C=C vibrations with a strong signal, i.e., 1625-1680 cm^{-1} in the molecular state, as listed in the web available "RAMAN Band Correlation Table", also due to the twice larger amounts of C=C bonds with sp^2 hybridization, there are more flat lines towards the top of the panel and less dispersion of the bands. These features are confirmed upon inspection of the Fig. 6c relevant to C_7, where the highest bands are flat with the highest line is found around 55 THz corresponding to the short C–C distance of 1.30 Å in the C=C=C subunit also identified in C_3H_4 propadiene (~1900 cm^{-1}).

8. Thermodynamic properties

The thermodynamic properties of novel carbon allotropes were calculated from the phonon frequencies using the statistical thermodynamic approach [37] on a high-precision sampling mesh in the Brillouin zone. The temperature dependencies of the heat capacity at constant volume (C_v) and entropy (S) are shown in Fig. 7 in comparison with available experimental C_p data for diamond [38,39]. For all three allotropes, the heat capacity and entropy are higher than those of diamond and increase in the C_5–C_6–C_7 series, which is to be expected due to the increasing openness of the crystal structures compared to diamond on the one hand, and the respective conducting versus insulator electronic properties, on the other hand.

9. Electronic band structures

The electronic band structures of three novel carbon allotropes were calculated using the all-electrons DFT-based augmented spherical method (ASW) [29]. The results are shown in Fig. 8. The bands (blue lines) develop along the main directions of the tetragonal Brillouin zone shown in Fig. 8d. The zero energy along the vertical axis is considered with respect to the Fermi level E_F, since all three allotropes C_5, C_6 and C_7 are metallic-like with no energy gap separating the valence band VB from the conduction band CB. Such behavior can be explained by the delocalized nature of the π electrons resulting from the presence of C(sp^2) atoms of the C=C and C=C=C subunits.

10. Conclusions

In the present work, the novel superhard tetragonal carbon allotropes C_5, C_6, and C_7 characterized with mixed sp^2 and sp^3 carbon hybridizations, were found to be cohesive and stable both mechanically (elastic constants and their combinations) and dynamically (phonon band structures). While C_5 and C_6 contain ethene-like >C=C< subunits, C_7 shows both ethene-like and propadiene-like >C=C=C< subunits, with signatures observed from the highest phonon frequencies correlating with Raman vibrations of ethene and propadiene molecules. The density decreases along the C_5–C_6–C_7 series due to the increasing openness of the structures and consequently leads to a decrease in the mechanical properties, in particular the Vickers hardness, which decreases from 90 GPa for C_5 to 79 GPa for C_7. The energy-volume equations of state show metastability of all three allotropes over the whole range of experimentally accessible pressures, but this does not exclude their possible formation under high pressure – high temperature conditions. Thermodynamically, the temperature dependencies of the heat capacity and entropy of all three allotropes were found to be higher than those of diamond due to the insulating electronic properties of the latter compared to the conducting C_5, C_6, and C_7 as identified from their electronic band structures. Delocalized π electrons of $C(sp^2)$ atoms present in the three new allotropes are considered responsible for their metallic-like conductivity.

Author Contributions: Conceptualization, S.F.M.; methodology, S.F.M. and V.L.S.; investigation, S.F.M. and V.L.S.; formal analysis, S.F.M. and V.L.S.; data curation, S.F.M. and V.L.S.; visualization, S.F.M. and V.L.S.; validation, S.F.M. and V.L.S.; resources, S.F.M.; writing – original draft preparation, S.F.M.; writing – review and editing, V.L.S. Both authors have read and agreed to the published version of the manuscript.

Funding: This research received no external funding.

Data Availability Statement: The data presented in this study are available on reasonable request.

Conflicts of Interest: The authors declare no conflict of interest.

References

1. Glass, C.W.; Oganov, A.R.; Hansen, N. USPEX – Evolutionary crystal structure prediction *Comput. Phys. Comm.* **2006**, *175*, 713-720.
2. Wang, Y.; Lv, J.; Zhu, L.; Ma, Y. CALYPSO: A method for crystal structure prediction. *Comput. Phys. Commun.* **2012**, *183*, 2063-2070.
3. Correiro, N.; Rizzi, R.; Settembre, R.G.; Del Buono, N.; Diacono, D. *CrystalMELA*: a new crystallographic machine learning platform for crystal system determination. *J. Appl. Cryst.* **2023**, *56*, 409-419.
4. Hoffmann, R.; Kabanov, A.A.; Golov, A.A.; Proserpio, D.M. Homo Citans and carbon allotropes: For an ethics of citation. *Angew. Chem. Int. Ed.* **2016**, *55*, 10962-10976; Samara Carbon Allotrope Database (http://www.sacada.info).
5. Matar, S.F.; Solozhenko. V.L. The simplest dense carbon allotrope: Ultra-hard body centered tetragonal C_4. *J. Solid State Chem.* **2022**, *314*, 123424.
6. Shevchenko, A.P.; Shabalin, A.A.; Karpukhin, I.Yu.; Blatov, V.A. Topological representations of crystal structures: generation, analysis and implementation in the *TopCryst* system. *Sci Technol Adv Mat.* **2022**, *2*, 250-265.
7. O'Keeffe M., Peskov M.A., Ramsden S.J., Yaghi O.M. The reticular chemistry structure resource (RCSR) database of, and symbols for, crystal nets. *Acc. Chem. Res.* **2008**, *41*, 1782-1789.
8. Wei, Q.; Zhang, Q.; Yan, H.; Zhang, M.; Wei, B. A new tetragonal superhard metallic carbon allotrope. *J. Alloys Compd.* **2018**, *769*, 347-352.
9. Fujii, Y.; Maruyama, M.; Cuong, N.T.; Okada S. Retraction: Pentadiamond: A hard carbon allotrope of a pentagonal network of sp^2 and sp^3 C atoms [Phys. Rev. Lett. 125, 016001 (2020)]. *Phys. Rev. Lett.* **2020**, *125*, 079901.
10. Yang, H.; Ma, Y.; Dai, Y. Progress of structural and electronic properties of diamond: a mini review. *Functional Diamond* **2021**, *1*, 150-159.
11. Hohenberg, P.; Kohn, W. Inhomogeneous electron gas. *Phys. Rev. B* **1964**, *136*, 864-871.
12. Kohn, W.; Sham, L.J. Self-consistent equations including exchange and correlation effects. *Phys. Rev. A* **1965**, *140*, 1133-1138.
13. Kresse, G.; Furthmüller, J. Efficient iterative schemes for ab initio total-energy calculations using a plane-wave basis set. *Phys. Rev. B* **1996**, *54*, 11169.
14. Kresse, G.; Joubert, J. From ultrasoft pseudopotentials to the projector augmented wave. *Phys. Rev. B* **1999**, *59*, 1758-1775.
15. Blöchl, P.E. Projector augmented wave method. *Phys. Rev. B* **1994**, *50*, 17953-17979.

16. Perdew, J.; Burke, K.; Ernzerhof, M. The Generalized Gradient Approximation made simple. *Phys. Rev. Lett.* **1996**, *77*, 3865-3868.

17. Press, W.H.; Flannery, B.P.; Teukolsky, S.A.; Vetterling, W.T. Numerical Recipes, 2nd ed.; Cambridge University Press: New York, USA, 1986.

18. Blöchl, P.; Jepsen, O.; Anderson, O. Improved tetrahedron method for Brillouin-zone integrations. *Phys. Rev. B* **1994**, *49*, 16223-16233.

19. Methfessel, M.; Paxton, A.T. High-precision sampling for Brillouin-zone integration in metals. *Phys. Rev. B* **1989**, *40*, 3616–3621.

20. Monkhorst, H.J.; Pack, J.D. Special k-points for Brillouin Zone integration. *Phys. Rev. B* **1976**, *13*, 5188-5192.

21. Gaillac, R.; Pullumbi, P.; Coudert, F.X. ELATE: an open-source online application for analysis and visualization of elastic tensors. *J. Phys.: Condens. Matter* **2016**, *28*, 275201.

22. Voigt, W. Über die Beziehung zwischen den beiden Elasticitätsconstanten isotroper Körper. *Annal. Phys.* **1889**, *274*, 573-587.

23. Mazhnik, E.; Oganov, A.R. A model of hardness and fracture toughness of solids. *J. Appl. Phys.* **2019**, *126*, 125109.

24. Chen, X.Q.; Niu, H.; Li, D.; Li, Y. Modeling hardness of polycrystalline materials and bulk metallic glasses. *Intermetallics* **2011**, *19*, 1275-1281.

25. Mukhanov, V.A.; Kurakevych, O.O.; Solozhenko, V.L. The interrelation between hardness and compressibility of substances and their structure and thermodynamic properties. *J. Superhard Mater.* **2008**, *30*, 368-378.

26. Mukhanov, V.A.; Kurakevych, O.O.; Solozhenko, V.L. Hardness of materials at high temperature and high pressure. *Phil. Mag.* **2009**, *89*, 2117-2127.

27. Lyakhov, A.O.; Oganov, A.R. Evolutionary search for superhard materials: Methodology and applications to forms of carbon and TiO_2. *Phys. Rev. B* **2011**, *84*, 092103.

28. Togo, A.; Tanaka, I. First principles phonon calculations in materials science, *Scr. Mater.* **2015**, *108*, 1-5.

29. Eyert, V. Basic notions and applications of the augmented spherical wave method. *Int. J. Quantum Chem.* **2000**, *77*, 1007-1031.

30. Momma, K.; Izumi, F. VESTA3 for three-dimensional visualization of crystal, volumetric and morphology data. *J. Appl. Crystallogr.* **2011**, *44*, 1272-1276.

31. Matar, S.F.; Solozhenko, V.L. Novel ultrahard sp^2/sp^3 hybrid carbon allotrope from crystal chemistry and first principles: Body-centered tetragonal C_6 ('neoglitter'). *Diam. Relat. Mater.* **2023**, *133*, 109747.

32. Brazhkin, V.V.; Solozhenko, V.L. Myths about new ultrahard phases: Why materials that are significantly superior to diamond in elastic moduli and hardness are impossible. *J. Appl. Phys.* **2019**, *125*, 130901.

33. Solozhenko, V.L; Matar, S.F. Prediction of novel ultrahard phases in the B-C-N system from first principles: Progress and problems. *Materials* **2023**, *16*, 886.

34. Munro, R.; Freiman, S.; Baker, T. Fracture toughness data for brittle materials. *NIST Interagency/Internal Report*, **1998**, No. 6153.

35. Matar, S.F.; Solozhenko, V.L. Crystal chemistry and *ab initio* prediction of ultrahard rhombohedral B_2N_2 and BC_2N. *Solid State Sci.* **2021**, *118*, 106667.

36. Birch, F. Finite strain isotherm and velocities for single-crystal and polycrystalline NaCl at high pressures and 300 K. *J. Geophys. Res.* **1978**, *83*, 1257-1268.

37. Dove, M.T. Introduction to lattice dynamics. Cambridge University Press: New York, USA, 1993.

38. DeSorbo, W. Specific heat of diamond at low temperatures. *J. Chem. Phys.* **1953**, *21*, 876-880.

39. Victor, A.C. Heat capacity of diamond at high temperatures. *J. Chem. Phys.* **1962**, *36*, 1903-1911.

Table 1 C_4-to-C_5 crystal structure transformation of tetragonal carbon allotropes.

Space group Topology	*tet*-C_4 [5] *I*-4*m*2 (No. 119) **dia**	Simple tetragonal C_4	*tet*-C_5 *P*-4*m*2 (No. 115) **3,4^2T1-CA**
a, Å	2.527	2.527	2.48
c, Å	3.574	3.574	4.99
Atomic positions	C1 (2a) 0, 0, 0 C2 (2d) ½, 0, ¼	C1a (½, ½, ½) → C1b (0, 0, 0) → C2a (½, 0, ¼) ⎤ → C2b (0, ½, ¾) ⎦	C1 (1c) ½, ½, ½ C2 (2e) 0, 0, ±z C3 (2g) 0, ½, ±z′

Table 2 Crystal structure parameters of new tetragonal carbon allotropes.

Space group Topology	C_5 *P*-4*m*2 (No. 115) **3,4^2T1-CA**	C_6 *I*-4*m*2 (No. 119) **tfa**	C_7 *P*-4*m*2 (No. 115) **tfa**
a, Å	2.480	2.456	2.563
c, Å	4.998	6.415	7.471
V_{cell}, Å^3	30.75	38.70	49.07
Density, g/cm^3	3.25	3.12	2.84
Shortest bond length, Å	1.46 / 1.50 / 1.55	1.44 / 1.51	1.30 / 1.45 / 1.53
Atomic positions	C1 (1c) ½, ½, ½ C2 (2e) 0, 0, 0.854 C3 (2g) 0, ½, 0.314	C1 (2c) 0, ½, ¼ C2 (4e) 0, ½, 0.888	C1 (1c) ½, ½, ½ C2 (2e) 0, 0, 0.903 C3 (2f) ½, ½, 0.326 C4 (2g) 0, ½, 0.210
E_{total}, eV	-43.29	-50.06	-58.07
E_{coh}/atom, eV	-2.06	-1.73	-1.69

N.B. E(C) = -6.6 eV. E_{coh}/atom (diamond) = -2.49 eV.

Table 3 Elastic constants (C_{ij}) of new tetragonal carbon allotropes (all values are in GPa).

	C_{11}	C_{12}	C_{13}	C_{33}	C_{44}	C_{66}
C_5	943	9	136	1194	198	337
C_6	784	19	135	1313	144	270
C_7	715	70	131	1286	119	268

Table 4 Mechanical properties of new tetragonal carbon allotropes compared with diamond: Vickers hardness (H_V), bulk modulus (B), shear modulus (G), Young's modulus (E), Poisson's ratio (ν), fracture toughness (K_{Ic})

	H_V				B		G_V	E_V	ν_V	K_{Ic}[‡]
	T[*]	LO[†]	MO[‡]	CN[§]	B_0[*]	B_V				
	GPa									$MPa \cdot m^{1/2}$
Diamond	98	90	100	93	445[**]		530[**]	1138[††]	0.074[††]	6.7[‡‡]
C_5 [#115]	90	81	49	45	410	405	333	784	0.177	7.1
C_6 [#119]	86	71	35	35	391	384	284	684	0.203	6.1
C_7 [#115]	79	62	30	31	360	376	260	634	0.219	5.8

[*] Thermodynamic model [26,26]

[†] Lyakhov-Oganov model [27]

[‡] Mazhnik-Oganov model [23]

[§] Chen-Niu model [24]

[**] Ref. 32

[††] Calculated from B_V and G_V using isotropic approximation

[‡‡] Ref. 35

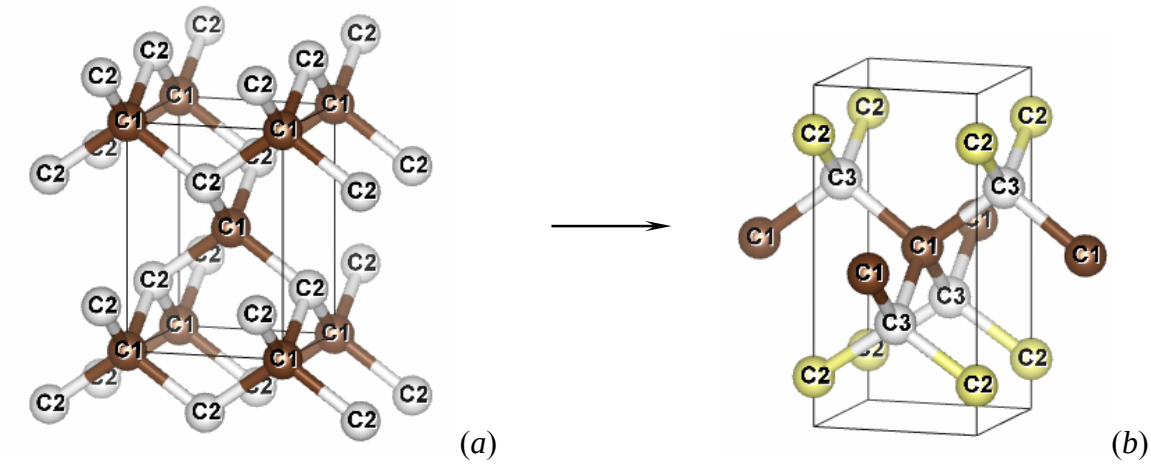

Figure 1 From *tet*-C_4 (*a*) to *tet*-C_5 (*b*) by changing the atomic positions. The carbon atoms numbers correspond to the numbering in Table 1.

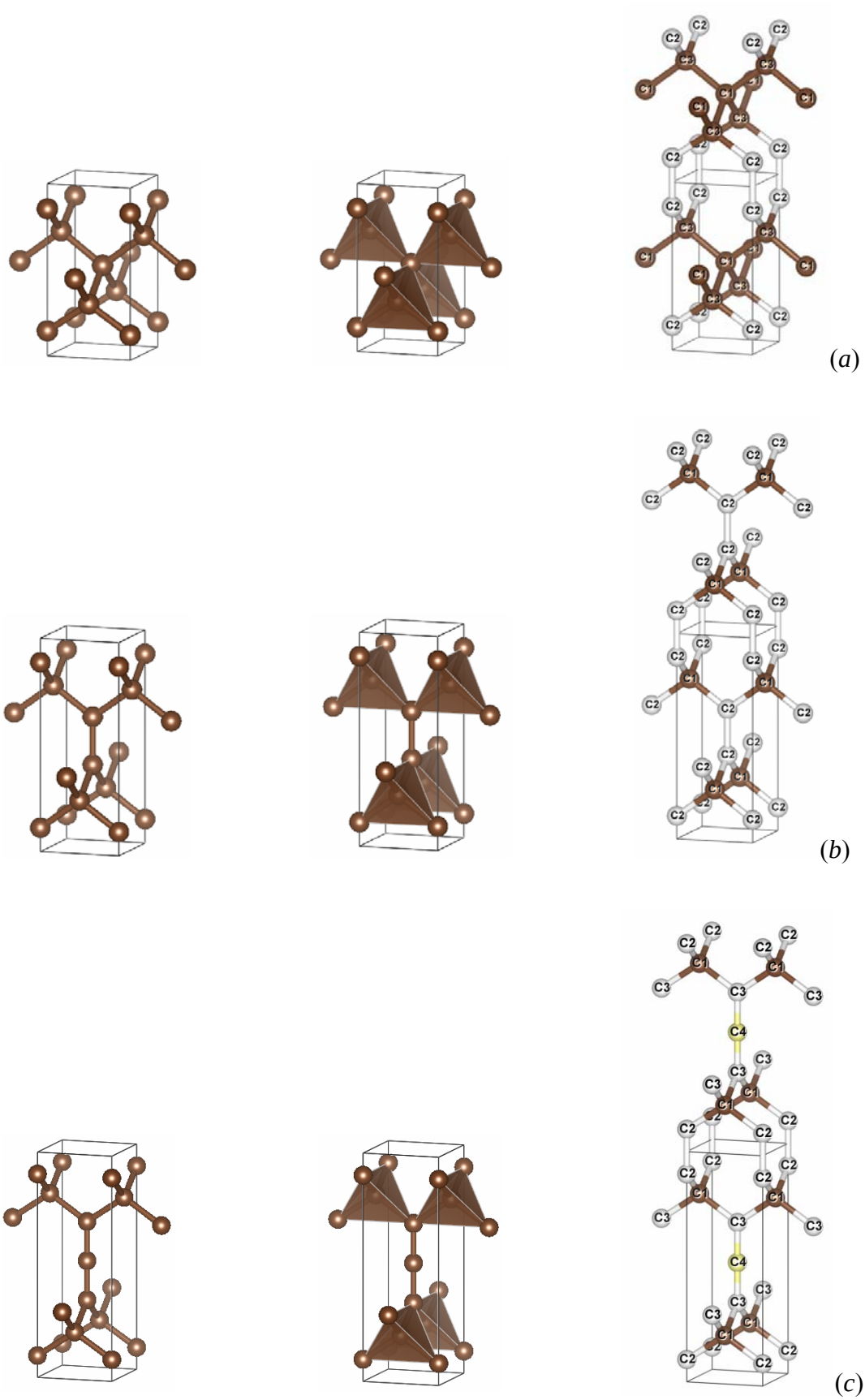

Figure 2 Crystal structures of new tetragonal carbon allotropes in three representations: ball-and-stick (left), polyhedral (middle), and double cells with atoms numbering as in Table 2: C_5 (*a*); C_6 (*b*); C_7 (*c*).

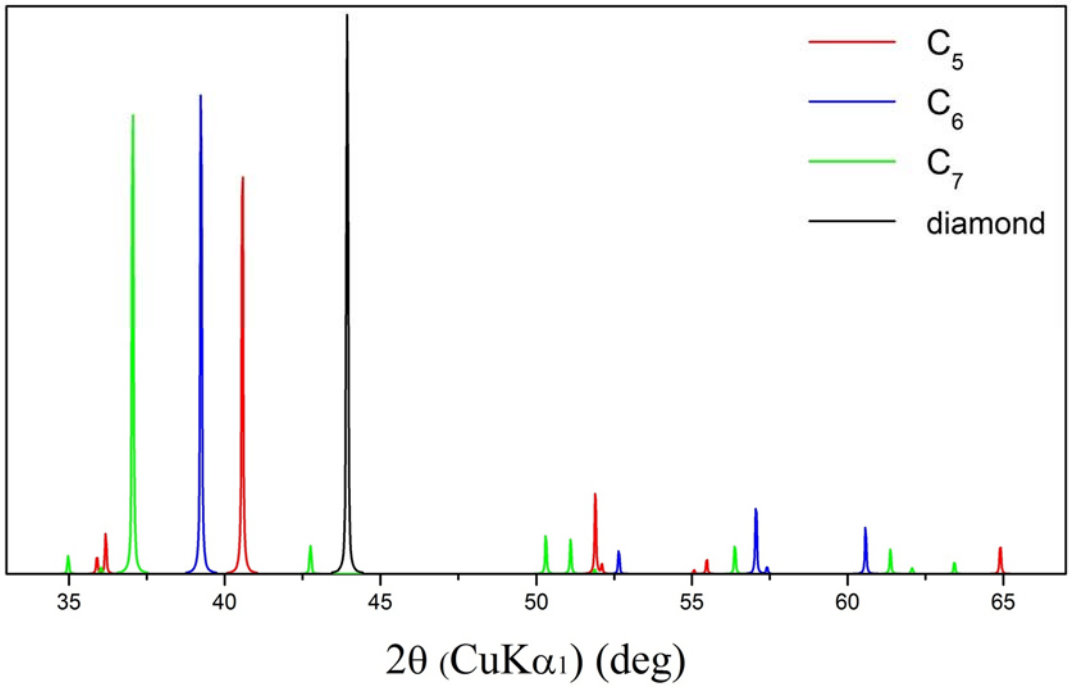

Figure 3 Simulated X-ray diffraction patterns of new tetragonal carbon allotropes.

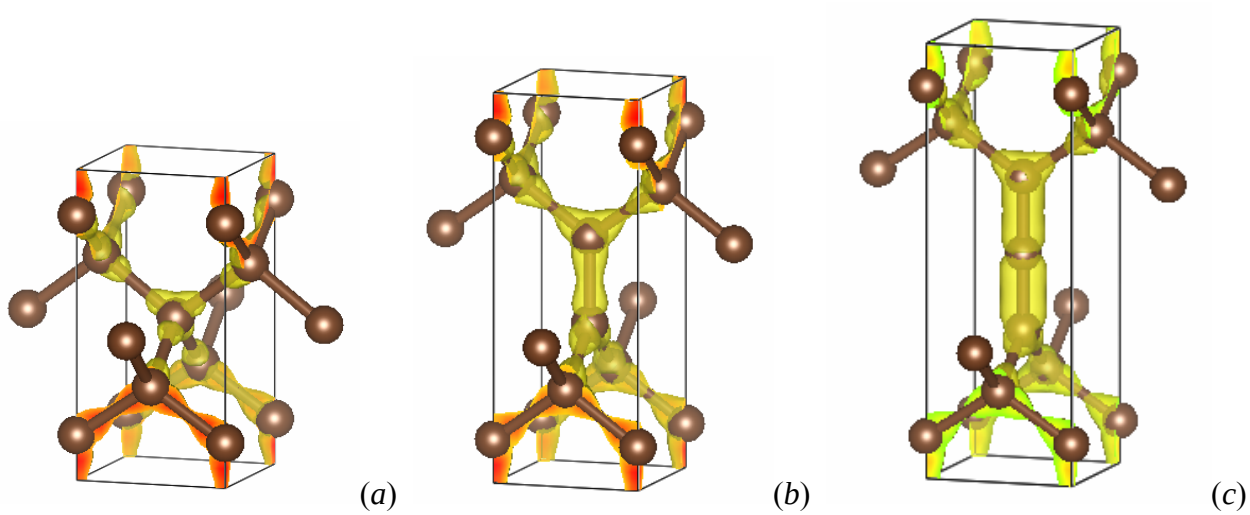

Figure 4 Charge density projections of tetragonal C_5 (*a*); C_6 (*b*); and C_7 (*c*).

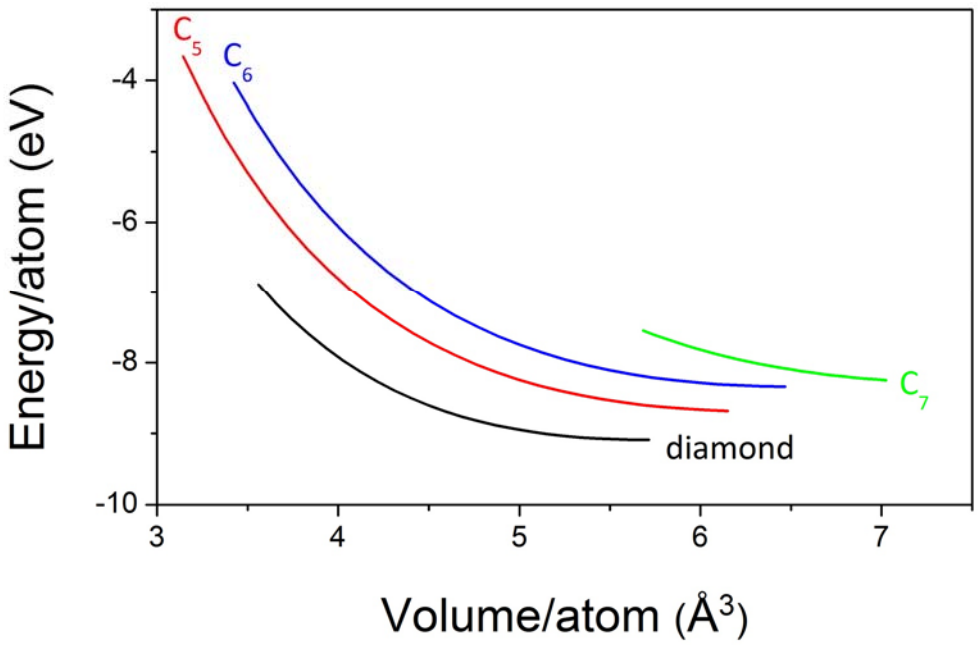

Figure 5 Calculated total energy per atom as a function of volume for new tetragonal carbon allotropes and diamond.

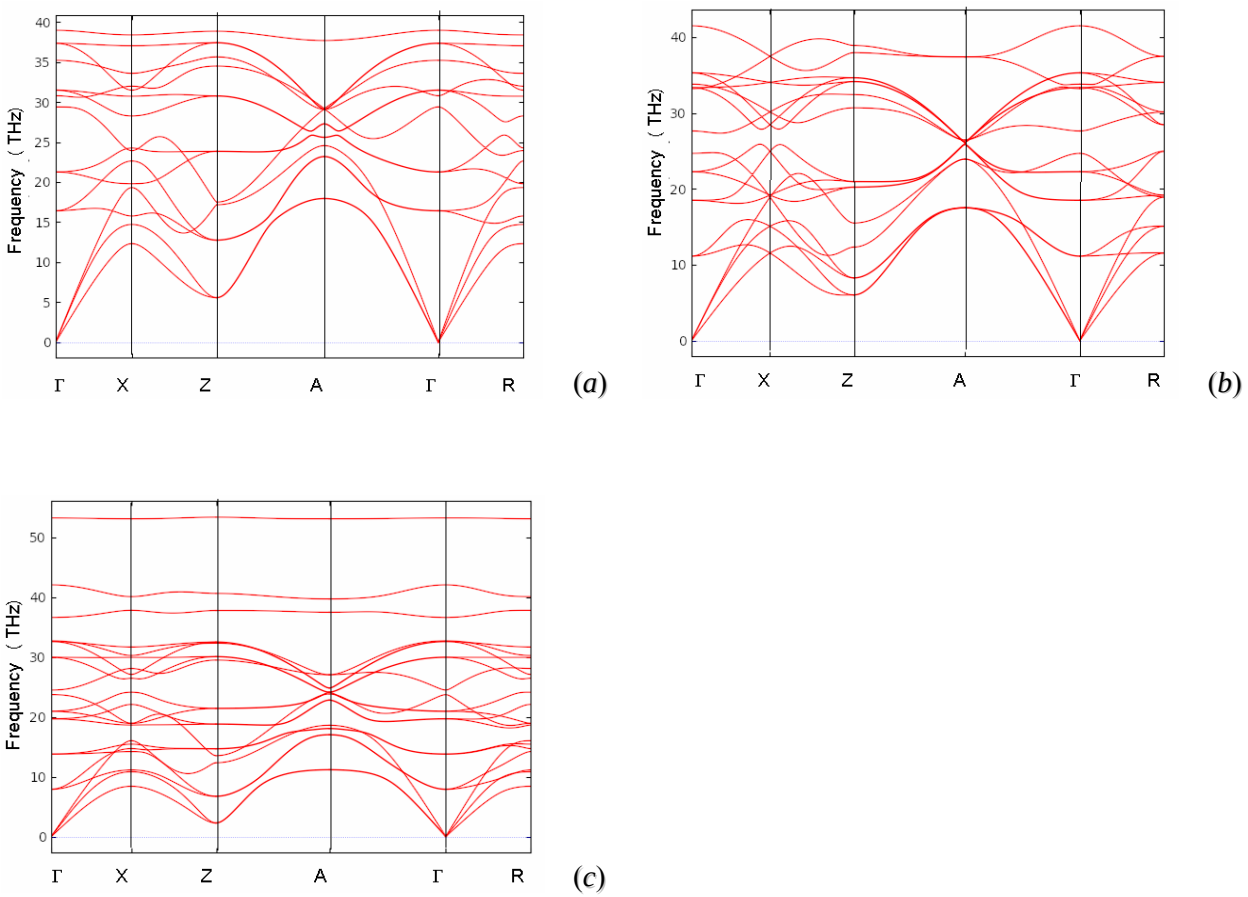

Figure 6 Phonon band structures of new carbon allotropes along the major directions of the simple tetragonal Brillouin zone: C_5 (*a*); C_6 (*b*); C_7 (*c*).

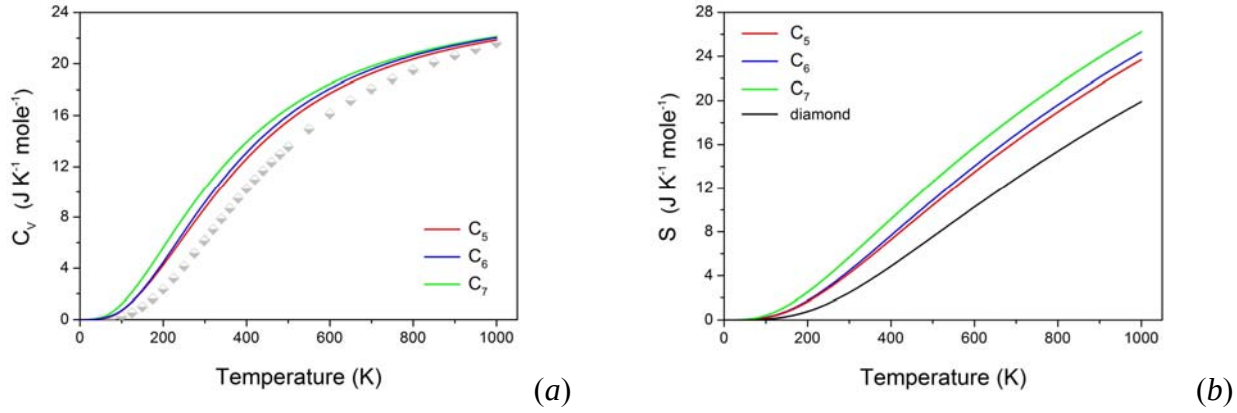

Figure 7 Heat capacities at constant volume (C_V) (*a*) and entropies (S) (*b*) of new tetragonal carbon allotropes compared to diamond. Experimental C_V data of diamond [38,39] are shown as gray symbols.

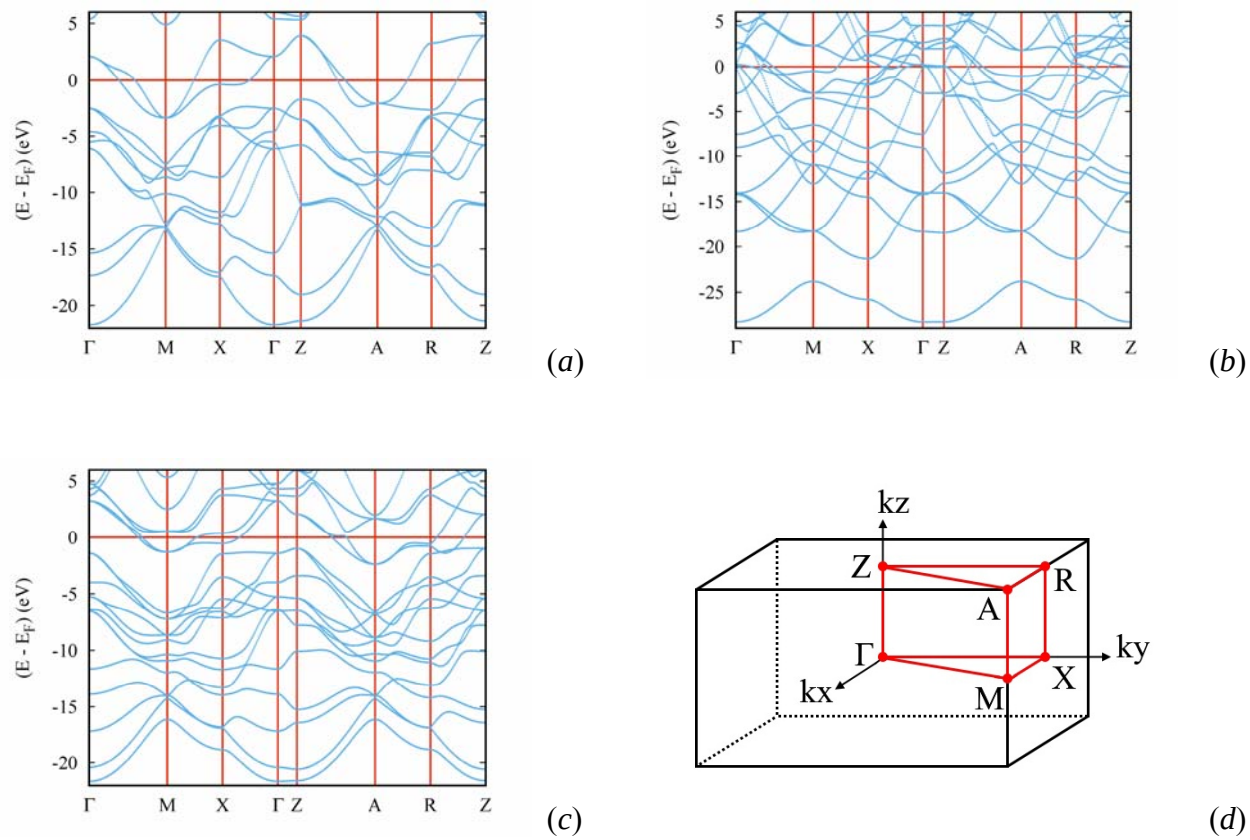

Figure 8 Electronic band structures of new tetragonal carbon allotropes: C_5 (*a*); C_6 (*b*); C_7 (*c*); the tetragonal Brillouin zone (*d*).